ЖУРНАЛ СТРУКТУРНОЙ ХИМИИ

2016. Том 57, № 5 *Июнь – июль* *С. 923 – 931*

UDC 541.6:547.13:546.72:546.76

EXPERIMENTAL AND THEORETICAL CHARACTERIZATION OF Fe_2Cr TRINUCLEAR-OXO-CENTERED COMPLEX WITH A CF_2ClCOO^- BRIDGE

A. Morsali, S.A. Beyramabadi, H. Chegini, N. Bozorgi, A. Moghadam-Elahabad

Department of Chemistry, Mashhad Branch, Islamic Azad University, Mashhad, Iran
E-mail: almorsali@yahoo.com; morsali@mshdiau.ac.ir; beiramabadi@yahoo.com; beiramabadi6285@mshdiau.ac.ir

Received November, 4, 2015

In this work, an atrinuclear-oxo-centered complex of the $CrFe_2$ type with the CF_2ClCOO^- bridging ligand is newly synthesized. The complex is characterized by experimental and theoretical methods. The optimized geometry and theoretical vibrational frequencies are computed using the density functional theory (DFT) method. Also, the AIM analysis was applied to study changes in topological parameters such as the electron density at critical points of all the bonds of the complex. In the optimized geometry of the complex, three metal ions form a trigonal-planar structure with a μ_3-O atom in its center. Each of M^{3+} metal ions has an octahedral coordination environment of oxygen atoms. The DFT results are in agreement with the experimental ones, confirming the validity of the optimized geometry for the complex.

DOI: 10.15372/JSC20160505

K e y w o r d s: synthesis, oxo-centered, trinuclear, carboxylate, CF_2ClCOO^-, DFT, AIM.

INTRODUCTION

In the structure of thetrinuclear-oxo-centered complexes, an oxygen atom is located at the center of the atriangle generated by three metal ions. Six carboxylate ligands bridge the three metal ions. Three monodentate ligands act as terminal ligands, too [1—4]. These complexes have been of interest in the viewpoints of electrochemical, structural, spectroscopic, and catalytic behavior [5—7].

The X-ray crystal structure of these compounds shows an essentially triangle arrangement of metal ions surrounding the central oxygen atom. Antiferromagnetic coupling between metal ions and the electron delocalization in which metal forms a mixed-valence cluster have been extensively investigated [8—11].

Herein, we report the synthesis and experimental characterization of a new trinuclear-oxo-centered complex with the $[Fe_2Cr(\mu_3\text{-}O)(\mu_2\text{-}CF_2ClCOO)_6(H_2O)_3]NO_3$ formula. In addition, the newly synthesized complex was theoretically investigated using DFT methods.

EXPERIMENTAL

Materials and methods. All the chemicals and solvents were purchased from Merck. They were used as received. Melting point of the complex was determined using an electrothermal 9100 melting point apparatus. The IR spectra were obtained on a Perkin Elmer 783 IR spectrophotometer. Percentage of the metals was obtained with a Shimadzu AA-670 GV/7 atomic absorption spectrophotometer.

Synthesis. A solution of $Fe(NO_3)_3 \cdot 9H_2O$ (2.69 g, 6.66 mmol) and $Cr(NO_3)_3 \cdot 6H_2O$ (1.33 g, 3.33 mmol) in 10 ml H_2O was added dropwise to a 20 mmol $CF_2ClCOOH$ solution neutralized with KOH in 10 ml H_2O. The brown solution was stirred for 2 h. After 3 weeks, the brown precipitate of

$[Fe_2Cr(\mu_3\text{-}O)(\mu_2\text{-}CF_2ClCOO)_6(H_2O)_3]NO_3$ was filtered and washed with cold water. (Yield: 2.28 g, 68.88 %; m.p. = 311 °C; calcd. (%): Fe 9.52, Cr 4.43; anal. (%): Fe 10.12, Cr 4.29.).

Computational details. All DFT calculations have been performed using the B3LYP functional [12] and 6-31G(*d*,*p*) basis sets. The Gaussian 98 program package [13] was used.

Geometries of the synthesized complex were optimized in the gas phase, which were confirmed to have no imaginary frequency of the Hessian. In the trinuclear-oxo centered complex of the carboxylic bridge (acetate group), Fe(III) ions have an octahedral surrounding with the high spin state: Fe(III) (S = 5/2) and Cr(III) (S = 3/2) [14].

Then, the vibrational frequencies were computed in the optimized geometry at the same computational level. Due to some reasons such as the use of finite basis sets and incomplete treatment of electron correlation, the DFT vibrational frequencies are usually higher than the experimental ones, which could be corrected by applying the scaling of wavenumbers [15]. The scale factor of 0.9614 was used for the correction of the computed wavenumbers.

The AIM topological analyses were carried out in accordance with Bader′s approach [16] using the AIMall package [17]. The DENSITY=CURRENT option was used to generate the wave function files.

RESULTS AND DISCUSSION

Geometry optimization. Percentages of metals in the synthesized complex were analyzed using the atomic absorption method. The results are in good agreement with the proposed formula $[Fe_2Cr(\mu_3\text{-}O)(\mu_2\text{-}CF_2ClCOO)_6(H_2O)_3]NO_3$ for the complex.

The optimized geometry of the complex with atom labeling is shown in Fig. 1. Some of DFT calculated structural parameters are gathered in Table 1. The DFT calculated structural parameters are in agreement with the experimentally data reported for the similar compounds [18—23].

In the $[Fe_2CrO(CF_2ClCOO)_6(H_2O)_3]^+$ cationic unit three metal atoms are bridged by the oxygen atom (O1) located at the center of the trigonal plane. The Fe2—Fe3—Cr4—O1 dihedral angle is –1.0°. Thus, the O1 atom and three metal ions are in the same plane.

The M—O1 bonds are shorter than the corresponding bonds of metal—O carboxylic bonds. The bond between the metal and H_2O terminal ligands is the longest metal—oxygen bond. Also, the Cr—O1 bond is shorter than Fe—O1 ones (Table 1).

Each of the metal atoms has an octahedral environment, where the μ_3-O1 atom occupies one of the octahedral positions. Four oxygen atoms of two carboxylic bridges occupy four coordination positions on the equatorial plane. The 6th coordination position is occupied by the H_2O terminal ligand, which is perpendicular to M—$O_{carboxylic}$ bonds.

In the octahedral environment around the metal ions, oxygen atoms of two carboxylic groups form a square planar geometry. For example, the O5—O8—O9—O10 and O17—O18—O19—O22 dihedral angles are –0.9° and –0.2°, respectively. However, metal ions do not have a regular octahedral environment and M—O bond lengths are not equal to each other. As for the M—O bond lengths, M—O1 is the strongest coordinative bond and M—OH_2 is the weakest one (Table 1).

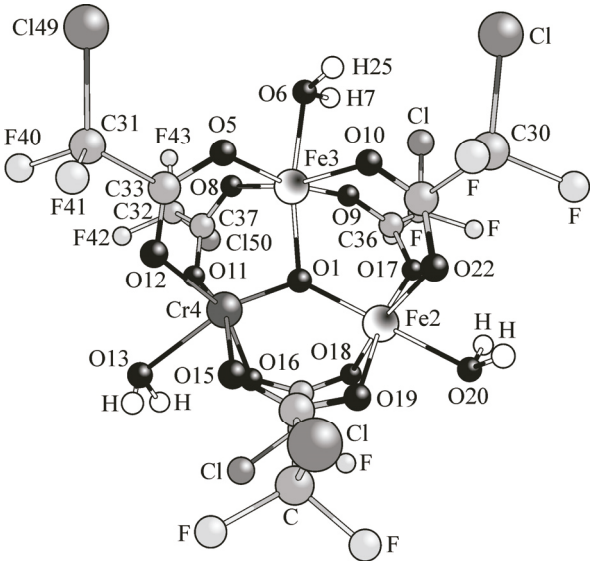

Fig. 1. Optimized geometry of $[Fe_2Cr(\mu_3\text{-}O)\cdot(\mu_2\text{-}CF_2ClCOO)_6(H_2O)_3]NO_3$ with atom labeling

Vibrational spectroscopy. Now a theoretical assignment of the spectra could be employed as an important tool for the identification of chemical compounds, especially analyzing the proposed geometries for compounds with an undetermined

Table 1

Important structural parameters of the investigated complex

Bond length, pm		Bond length, pm		Angle, deg.		Angle, deg.	
Cr4—O1	164.6	Fe3—O8	194.4	Cr4—O1—Fe2	130.4	O5—Fe3—O8	91.4
Fe2—O1	185.5	Fe3—O10	196.4	Cr4—O1—Fe3	107.4	O5—Fe3—O9	168.2
Fe3—O1	195.1	C33—O12	127.7	Fe3—O1—Fe2	122.1	O5—Fe3—O6	86.3
Cr4—Fe2	318.0	C33—O12	124.9	O1—Cr4—O15	93.1	O10—Fe3—O6	81.3
Cr4—Fe3	290.5	C33—C31	152.2	O1—Cr4—O12	111.6	Cr4—O12—C33	125.5
Fe3—Fe2	333.1	C31—Cl49	179.4	O1—Cr4—O13	164.2	Fe3—O5—C33	126.1
Cr4—O13	216.3	C31—F41	140.9	O15—Cr—O12	85.7	O5—C33—C31	121.0
Cr4—O15	202.9	Fe3—O6	200.6	O15—Cr—O16	90.7	O5—C33—C31	113.0
Cr4—O12	195.5	O1—H25	97.2	O15—Cr—O11	161.9	C33—C31—Cl49	114.8
Fe3—O5	194.6			O1—Fe3—O6	168.6	C33—C31—F41	108.3
				O1—Fe3—O5	101.8	Cl49—C31—F41	107.9
				O1—Fe3—O10	91.1	F40—C31—F41	108.4
				O5—Fe3—O10	86.3	Fe2—Cr4—Fe3	66.2

Dihedral angle, deg.		Dihedral angle, deg.		Dihedral angle, deg.	
Fe2—Fe3—Cr4—O1	–1.0	O11—O12—Cr4—O15	–162.5	Fe3—O5—C33—C31	–172.3
O5—O8—O9—O10	–0.9	Fe2—O22—O10—Fe3	6.4	O5—C33—C31—Cl49	16.9
O5—O8—O9—Fe3	8.1	Fe2—O19—O15—Cr4	16.5	O5—C33—C31—F41	–103.6
O11—O12—O15—O16	–4.8	Fe3—O5—O12—Cr4	15.1	Cr4—O5—C33—C31	–169.5

structure [23—32]. Selected vibrational frequencies of the newly synthesized oxo-complex are assigned theoretically. The obtained results are gathered in Table 2.

An important diagnostic for the oxo complexes is the energy value of intense bands in the 1350—1480 and 1550—1710 cm^{-1} regions of the IR spectra, which are related to the symmetrical and asymmetrical C=O stretching modes of the —CO_2 moieties [22, 32, 33]. The intense bands at 1427 and 1603 cm^{-1} in the IR spectra are attributed to υ_{sym}(C=O) and υ_{asym}(C=O) stretching vibrations, respectively (Table 2). A weak band at 857 cm^{-1} and a medium band at 1211 cm^{-1} are attributed to C—Cl and C—F stretching modes, respectively.

In the 3600—2000 cm^{-1} region of the IR spectra, the overlap of stretching vibrations of the O—H and C—H bonds leads to band broadening [23, 25—33, 35]. For the investigated complex, the deconvolution of a broad and strong band at 3489 cm^{-1} is given in Table 2.

Table 2

Selected experimental and DFT *calculated* IR *vibrational frequencies* (cm^{-1}) *of the oxo complex*

Experimental frequencies	Calculated frequencies	Vibrational assignment
508 (w)	489	υ(M—O)
657 (m)	625	$\delta_{wagging}$(O—H) H_2O
857 (w)	895	υ(C—Cl)
1211 (m)	1183	υ(C—F)
1427 (s)	1411	υ_{sym}(C=O)
1603 (vs)	1668	υ_{asym}(C=O)
3489 (br, s)	3602—3622	υ_{sym}(O—H)
	3702—3728	υ_{asym}(O—H)

Quantum theory of atoms in molecules (QTAIM). The bond paths, atomic basins and their boundaries can be defined from the topology of this field [36, 37]. The superposition of the bond paths and atomic boundaries defined by the gradient vector field on the electron density distribution is shown with an accompanying graph. The bonding that physically presents between atoms is also a sign of an accompanying energetic stabilization because every bond path is reflected by a virial path that links the similar nuclei along which the electron potential energy density is maximally stabilizing [38]. Thus, each molecular graph is accompanied by a virial graph represen-

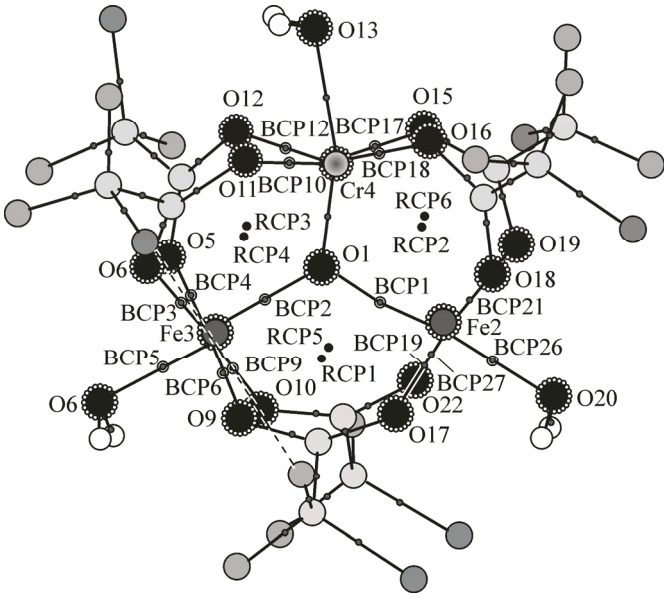

Fig. 2. QTAIM molecular graph of the titled oxo complex

ting the presence of a corresponding set of lines defined in real space. The virial graph describes a decrease in the energy related with the structure formation defined by the molecular graph. The presence of a bond path always infers stabilization [39].

The molecular graphs for the entitled-oxo complex (Fig. 2) indicate that three metal ions are linked by a bond path to the central oxygen atom (O1), causing the formation of six-membered chelate rings. The presence of RCP in these rings is a sign of the stabilization effect of M—O bonds in these rings on both sides of metal atoms. RCP is a point of the minimum electron density within the ring surface and the maximum on the ring line [40].

Description of metal—ligand bonding in terms of pair and bond indices. Enumerating the number of localized and shared electron pairs. The molecular graphs for the oxo-centered complexes need analyzing. The chemical structures of metal atoms bound to the central oxygen atom, oxygen atoms of bidentate ligands, and a water molecule are determined by a bond linking the metal ions to six oxygen atoms.

The bidentate-carboxylic ligands have two oxygen atoms with electron pairs located on the oxygen atom and increasing the charge transfer in the rings. From the 2D countermap, it can be seen that the negative charge, presented by a broken red line, on the metal atoms and the central oxygen (O1 atom) has been delocalized because of the ring resonance and the structure in the presence of water molecules bonded to metal ions have delocalized positive charge more over the water ligands.

Nevertheless, QTAIM comes up with an answer to the problem of counting the number of electrons shared between atom pairs and the number of those localized on each of them. The electron localization index for atom A, $|F(\mathrm{A},\mathrm{A}) = \lambda(\mathrm{A})|$, determines the number of electrons localized in the basin of atom A.

It is obvious that its limiting value $N(\mathrm{A})$ is the population of atom A, in which one $N(\mathrm{A})/2$ pair of electrons is localized on A.

$$N(\mathrm{A}) = \lambda(\mathrm{A}) + \left(\frac{1}{2}\right)\sum_{\mathrm{B}\neq\mathrm{A}} \delta(\mathrm{A},\mathrm{B}). \qquad (1)$$

The percent localization of electrons on A is obtained by $l(\mathrm{A}) = \dfrac{\lambda(\mathrm{A})}{N(\mathrm{A})} \times 100\%$. The sum of the localization of electron percentage can approach 99 %.

The electron delocalization between two atomic basins A and B is given by the following expression $F(\mathrm{A},\mathrm{B})$ [41]

$$F(\mathrm{A},\mathrm{B}) = -\sum_{i,j} S_{i,j}(\mathrm{A}) S_{i,j}(\mathrm{B}). \qquad (2)$$

It is noteworthy that $F(\mathrm{A},\mathrm{B})$ is equivalent to $F(\mathrm{B},\mathrm{A})$ and their sum, which is called the delocalization index $\delta(\mathrm{A},\mathrm{B})$, is a factor for the degree of exchange between electrons on A and B [42]. The $\delta(\mathrm{A},\mathrm{B})$ values for Fe2 and Fe3 as atom A and water molecule O and also bidentate ligand oxygen atoms can be obtained from the data of Tables 3 and 4. The presented data show that the bonding of water molecules to the metal ions seems to be non-covalent and the bonding of carboxylic oxygen atoms

can be partial-covalent. Due to the uniform electron density distribution and a great similarity and symmetry of the complex, the bond order in the metal bonding to oxygen atoms of ligands is equal on both sides of the metal atom.

Recovery of the Lewis model in the delocalization indices. The equal distribution of one Lewis pair between A and B necessarily needs that $\lambda(A) = \lambda(B) = 0.5$ and $\delta(A,B) = 1.0$ and, therefore, $\delta(A,B) = 1$, 2, or 3 for the corresponding numbers of shared electron pairs. If the sharing of a pair is accompanied by an electron charge transfer from A to B, then the density localization in the atomic basins given and $\delta(A,B) < 1.0$, assuming the values of ionic interactions, is <0.2. The $\delta(A,B)$ value for an A—B molecule is a function of the square of the transferred charge and reduces with charge transfer from values of one, two, and three. Hence, a value of $\delta(A,B) < 1$ for an atom pair connected by a bond path does not mean that less than an electron pair is contributed between A and B, but that they are unfairly shared. In addition, $\delta(A,B)$ for a pair equally shared between two atoms in a molecule is fairly less than unity because the electrons on A and B are more delocalized over other atoms in the system.

At any rate, the $\delta(A,B)$ value always presents the number of delocalized or exchanged electrons between the basins of A and B. The exchange or the number of electron pairs between the bonding atoms is a mechanism having the key role in the understanding of the covalent bond.

Therefore, the delocalization index $\delta(A,B)$ determining the number of electron pairs exchanged between two atomic basins can be used to judge about the degree of covalency.

T a b l e 3

Electron localization and delocalization indices (*in* e^- *units*)

Atom	q(A)	LI(A)	LI(A), %	$\delta(A,A')/2$	$\delta_{Bond}(A,A')/2$	$\delta_{NonBond}(A,A')/2$	N(A)
Fe3	1.37	22.95	93.18	1.68	1.39	0.29	24.63
Cr4	1.85	20.02	90.42	2.12	1.73	0.39	22.15
Fe2	1.35	23.00	93.31	1.65	1.36	0.28	24.65
O1	–0.89	7.44	83.71	1.45	1.21	0.24	8.89
O10	–1.11	7.96	87.39	1.15	0.78	0.37	9.11
O11	–1.13	8.00	87.61	1.13	0.74	0.39	9.13
O12	–1.15	8.01	87.49	1.15	0.73	0.41	9.15
O13	–1.11	8.20	89.99	0.91	0.74	0.17	9.11
O15	–1.10	7.95	87.43	1.14	0.78	0.36	9.10
O16	–1.09	7.94	87.32	1.15	0.78	0.37	9.09
O17	–1.15	8.00	87.46	1.15	0.77	0.38	9.15
O18	–1.11	7.96	87.36	1.15	0.81	0.34	9.11
O19	–1.09	7.94	87.29	1.16	0.81	0.35	9.09
O22	–1.14	7.99	87.46	1.15	0.77	0.38	9.14
O5	–1.08	7.94	87.44	1.14	0.80	0.34	9.08
O6	–1.08	8.14	89.67	0.94	0.81	0.12	9.08
O8	–1.10	7.95	87.43	1.14	0.79	0.35	9.10
O9	–1.11	7.96	87.37	1.15	0.78	0.37	9.11
C27	1.64	2.73	62.59	1.63	1.50	0.13	4.36
C33	1.66	2.71	62.52	1.63	1.51	0.12	4.34
C34	1.66	2.71	62.45	1.63	1.51	0.12	4.34
C35	1.64	2.73	62.52	1.64	1.51	0.13	4.36
C36	1.66	2.71	62.47	1.63	1.51	0.12	4.34
C37	1.64	2.72	62.43	1.64	1.51	0.12	4.36

Table 4

Topological properties at the BCP *of* M—O *and* O—C *bonds in carboxylic ligand* $|q(A,B)|$ *and* $\delta(A,B)$ *are in* e^- *units*, *bond path length* (BPL) *is in* Bohr *units* ρ, $\nabla^2\rho$, G, V, H *values are in* a.u.

BCP #	$\|q(A,B)\|$	$\delta(A,B)$	BPL	Atoms	ρ	$\nabla^2\rho$	G	V	H	$-G/V$	G/ρ
1	0.174	0.486	3.773	O1—Fe2	0.080	0.475	0.123	–0.127	–0.004	0.967	1.535
2	0.170	0.567	3.546	O1—Fe3	0.097	0.782	0.202	–0.208	–0.006	0.969	2.085
3	0.543	1.362	3.113	O1—Cr4	0.229	0.806	0.344	–0.486	–0.142	0.707	1.499
4	0.318	0.457	3.760	Fe3—O5	0.076	0.535	0.134	–0.134	–0.000	0.998	1.766
5	0.125	0.393	3.900	Fe3—O6	0.064	0.448	0.110	–0.107	0.003	1.023	1.703
6	0.346	0.457	3.759	Fe3—O9	0.077	0.530	0.134	–0.135	–0.001	0.992	1.734
9	0.341	0.455	3.763	Fe3—O10	0.076	0.531	0.133	–0.134	–0.001	0.996	1.755
10	0.366	0.413	3.862	Cr4—O11	0.074	0.406	0.105	–0.107	–0.003	0.972	1.408
12	0.363	0.40	3.845	Cr4—O12	0.074	0.410	0.105	–0.107	–0.002	0.978	1.426
15	0.113	0.278	4.093	Cr4—O13	0.055	0.247	0.061	–0.060	0.001	1.019	1.094
17	0.344	0.503	3.729	Cr4—O15	0.091	0.487	0.132	–0.143	–0.010	0.927	1.454
18	0.350	0.502	3.727	Cr4—O16	0.091	0.471	0.129	–0.140	–0.011	0.922	1.408
19	0.364	0.430	3.779	Fe2—O17	0.074	0.514	0.128	–0.128	0.000	1.001	1.744
21	0.291	0.477	3.737	Fe2—O18	0.079	0.558	0.141	–0.142	–0.001	0.992	1.787
24	0.289	0.483	3.734	Fe2—O19	0.079	0.558	0.141	–0.142	–0.002	0.990	1.776
26	0.131	0.413	3.854	Fe2—O20	0.068	0.472	0.116	–0.115	0.002	1.014	1.703
27	0.366	0.438	3.770	Fe2—O22	0.075	0.518	0.130	–0.130	–0.000	0.998	1.736
22	0.741	1.056	2.414	O16—C27	0.352	–0.386	0.456	–1.008	–0.552	0.452	1.294
34	0.816	1.136	2.360	O18—C27	0.378	–0.328	0.531	–1.144	–0.613	0.464	1.405
42	0.791	1.064	2.391	O12—C33	0.360	–0.338	0.486	–1.056	–0.570	0.460	1.348
13	0.765	1.138	2.374	O5—C33	0.373	–0.389	0.505	–1.107	–0.602	0.456	1.352
41	0.775	1.099	2.374	O22—C34	0.370	–0.349	0.507	–1.101	–0.594	0.460	1.369
29	0.768	1.107	2.393	O10—C34	0.364	–0.406	0.477	–1.056	–0.579	0.452	1.313
39	0.753	1.061	2.407	O15—C35	0.358	–0.427	0.459	–1.024	–0.565	0.448	1.282
40	0.802	1.130	2.372	O19—C35	0.373	–0.358	0.512	–1.113	–0.601	0.460	1.373
20	0.761	1.103	2.394	O9—C36	0.364	–0.417	0.475	–1.054	–0.579	0.451	1.305
37	0.783	1.101	2.371	O17—C36	0.371	–0.322	0.514	–1.109	–0.595	0.464	1.388
43	0.762	1.070	2.409	O11—C37	0.356	–0.427	0.455	–1.016	–0.561	0.448	1.276
11	0.779	1.137	2.373	O8—C37	0.372	–0.369	0.508	–1.108	–0.600	0.458	1.363

In the AIM theory the term ″shared interaction″ is used instead of the term ″covalency″. What is important is that the delocalization index, as the expectation value for the exchange operator over two atomic basins, supplies a quantitative measure for the number of exchanged electrons in any given interaction, consequently, quantifying the covalency for those who are interested in retaining the term. The $\delta(A,B)$ and $L(A)$ data for Fe, Cr, O1, C and O of carboxylic groups and oxygen atoms of H_2O ligands are presented in Table 4.

According to Table 4, the localized charge on the Fe2 and Fe3 atoms is equal to each other, which means that the type and binding order of two Fe atoms are similar.

Fewer localization electrons on the Cr atom than on Fe atoms express the idea that the Cr—O1 bond can be stronger than Fe—O1 ones. In the next section, the order of each M—O1 bond is explained.

BCP based description. The BCP data are shown in Table 4. A detailed discussion about the BCP properties of metal—ligand and metal—metal bondings are presented by Macchi and Sironi [42]. This discussion includes a summary of BCP properties for prototype molecules and tables of

Fig. 3. 2D and 3D isosurfaces of $\nabla^2\rho$

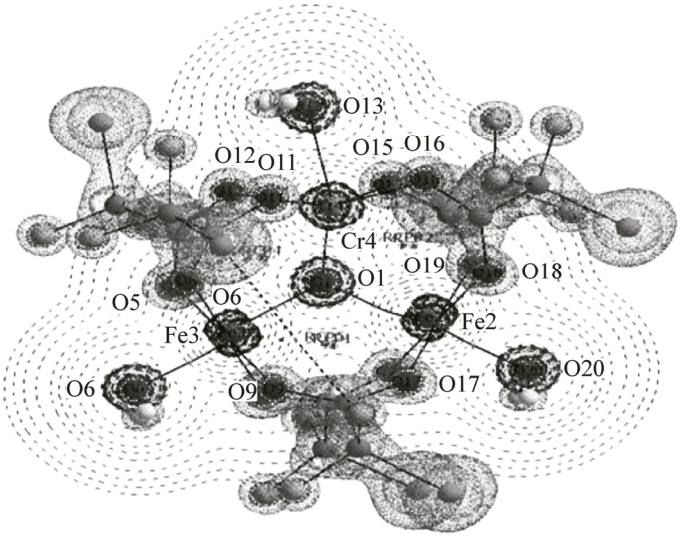

characteristics of the types bonding between light and heavy metal atoms. In this section, the basic features describing the bonding in the investigated oxo-complex are discussed. The delocalization indices for M—O_{eq} and M—O_{ax} bonding (in the bidentate ligand and water molecules, respectively) are typical of the shared interaction. The electron density ρ(r) is one of the main properties of the bond and the small ρ values for M—O_{eq} and M—O_{ax} bonds is a reflection of the electron density delocalization over multiple bonds between the metal atom and the central oxygen atom. The energy density *H*, for example, for an interaction which is shared, is negative [43] but smaller than that for a bonded interaction which is individually shared, and also the *G*/ρ ratio, in which *G* is the kinetic energy density, has a greater value than 0.5 for all metal—oxygen bonds (M—O_{eq} and M—O_{ax}), while for shared interactions it is <1.0.

The combination of BCP indices, pretty low ρ values, small negative values for *H* with *G*/ρ ~ 1, and also small positive values for $\nabla^2\rho$ values coupled with noteworthy electron delocalization, are exceptional to bonding to a metal atom [42, 44]. Regarding ρ and $\nabla^2\rho$ values and also using the counter map *via* $\nabla^2\rho$, we can state that resonance or locating electron over it occur within this region (Fig. 3). $q(A|B)$ is the absolute value of transferred charge between two atoms.

This charge is along with the bond length, and from the Table 4 data its magnitude is less than 0.2 for the O1—Fe covalent bond, but for the strong interaction of O1—Cr it is 0.5429. With this information in hand and also related values, it can be considered as a metal bond for O1—Fe bonds.

From the comparison of O1—Cr and O1—Fe bond lengths it is obvious that the O1—Cr bond is stronger than O1—Fe bonds. The analysis of Table 4 data shows that the O1—Cr bond is a dipolar bond.

A dative covalent bond is provided by the intramolecular interaction between the central oxygen atom as a Lewis base with $\delta(A,B) = 1.3623$ and a Cr atom as a Lewis acid.

With notice to the obtained values from Table 4 and regarding the fact that for all $\nabla^2\rho$ negative values the interaction is undoubtedly totally covalent, the following statement can be concluded. If both $\nabla^2\rho$ and *H* are simultaneously positive, it means that the interaction is non-covalent. If $\nabla^2\rho$ is positive while *H* is negative and $-G/V$ is smaller than 1, then the interaction nature is considered as partly covalent [45]. From the related values of the metal—OH_2 bonding and its positive values, it can be concluded that its bonding is non covalent. The bond lengths presented in Table 4 show that the length of a non-covalent bond is about 4.00, and that for a dipolar bond is 3.1127, which confirms the mentioned argument.

CONCLUSIONS

In this work, the atrinuclearoxo-centered complex with the formula $[Fe_2Cr(\mu_3\text{-}O)(\mu_2\text{-}CF_2ClCOO)_6 \times \times (H_2O)_3]NO_3$ has been newly synthesized. The complex was characterized by experimental and theoretical methods. The optimized geometry and IR vibrational frequencies of the complex were calculated using the valuable DFT methods.

In the optimized structure of the complex, three M^{3+} metal ions form a triangle with μ_3-O located at the center of this trigonal plane. Six oxygen atoms are coordinated to each metal atom, giving rise to an octahedral environment around the Fe^{3+} and Cr^{3+} metal ions. The oxygen atoms of the CF_2ClCOO^-

carboxylic bridges occupy four equatorial positions in the square manner. The μ_3-O1 atom and the oxygen atom of a terminal H_2O ligand are perpendicular to this square and occupy *trans* positions in the octahedral structure. The O1—Cr bond is stronger than O1—Fe bonds.

The calculated results are in agreement with the experimental ones, confirming the suitability of the optimized geometries. The DFT data could be used for the identification of similar compounds.

We gratefully acknowledge the financial support from the Islamic Azad University, Mashhad Branch.

REFERENCES

1. *Flynn C.M. Jr.* // Chem. Rev. – 1986. – **84**. – P. 31 – 41.
2. *Jang N.G., Kaji K., Sorei M., Wittebort R.J., Geib S.J., Rheingold A.L., Hendrickson D.N.* // Inorg. Chem. – 1990. – **29**. – P. 3547 – 3556.
3. *Vincent J.B., Chang H.R., Folting K., Human J.C., Christou G., Hendrickson D.N.* // J. Am. Chem. Soc. – 1987. – **109**. – P. 5703 – 5711.
4. *Sasaki Y., Nagasawa A., Tokiwa-Yamamoto A., Nagasawa A., Ito T.* // Inorg. Chim. Acta. – 1993. – **212**. – P. 175 – 182.
5. *Earnshaw A., Figgis B.N., Lewis J.* // J. Chem. Soc., A. – 1966. – P. 1656 – 1663.
6. *Cotton F.A., Wang W.* // Inorg. Chem. – 1982. – **21**. – P. 2675 – 2678.
7. *Vemura S., Spencer A., Wilkinson G.* // J. Chem. Soc., Dalton Trans. – 1973. – **23**. – P. 2565 – 2571.
8. *D'Alessandro D.M., Keene F.R.* // Chem. Rev. – 2006. – **106**. – P. 2270 – 2298.
9. *Liu J.Y., Li Y.S., Liu J.Y., Li Z.S.* // J. Mol. Cat. A: Chem. – 2006. – **244**. – P. 99 – 104.
10. *Chang S.C., Jeffery S.A.* // Acta Crystallogr. – 1970. – **B26**. – P. 673.
11. *Wilson C., Inversen B.B., Overgard J., Larsen F.K., Wu G., Palli S.P., Timco G.A., Gerbeleu N.V.* // J. Am. Chem. Soc. – 2000. – **122**. – P. 11370 – 11379.
12. *Lee C., Yang W., Parr R.G.* // Phys. Rev. B. – 1988. – **37**. – P. 785 – 789.
13. *Frisch M.J. et al*. Gaussian 98, Revision A.7. – Pittsburgh, PA: Gaussian Inc., 1998.
14. *Turte K.I., Shova S.G., Meriacre V.M., Gdaniec M., Simonov Yu.A., Lipkowski J., Bartolome J., Wagner F., Filoti G.* // J. Struct. Chem. – 2014. – **43**. – P. 108 – 117.
15. *Young D.C*. Computational Chemistry: A Practical Guide for Applying Techniques to Real-World Problems. – John Wiley & Sons, 2001.
16. *Bader R.F.W*. Atoms in Molecules: A Quantum Theory. – Oxford, U. K.: Clarendon Press, 1994.
17. *Biegler-König F., Schönbohm J., Bayles D.* // J. Comput. Chem. – 2001. – **22**. – P. 545 – 559.
18. *Raptopoulou C.P., Psycharis V.* // Inorg. Chem. Commun. – 2008. – **11**. – P. 1194 – 1197.
19. *Houston J.R., Olmstead M.M., Casey W.H.* // Inorg. Chem. – 2006. – **45**. – P. 7799 – 7805.
20. *Zhang K.-L., Shi Y.-J., Gao S., Dai Y.-D., Yu K.-B., You X.-Z.* // Inorg. Chem. Commun. – 2004. – **7**. – P. 584 – 587.
21. *Li J., Zhang F., Shi Q., Wang J., Wang Y., Zhou Z.* // Inorg. Chem. Commun. – 2002. – **5**. – P. 51 – 55.
22. *Figuerola A., Tangoulis V., Ribas J., Hartl H., Bru1dgam I., Maestro M., Diaz C.* // Inorg. Chem. – 2007. – **46**. – P. 11017 – 11024.
23. *Beyramabadi S.A., Morsali A., Pordel M., Chegini H., Khashi M., Ahmadi I., Poorzaki M.* // J. Struct. Chem. – 2015. – **56**. – P. 1253 – 1261.
24. *Avcı D., Atalay Y., Şekerci M., Dinçer M.* // Spectrochim. Acta, Part A. – 2009. – **73**. – P. 212 – 217.
25. *Li L., Cai T., Wang Z., Zhou Z., Geng Y., Sun T.* // Spectrochim. Acta, Part A. – 2014. – **120**. – P. 106 – 118.
26. *Beyramabadi S.A., Eshtiagh-Hosseini H., Housaindokht M.R., Shirzadi S., Morsali A., Naseri M.A.* // J. Struct. Chem. – 2013. – **54**. – P. 1055 – 1062.
27. *Eshtiagh-Hosseini H., Housaindokht M.R., Beyramabadi S.A., Beheshti S., Esmaeili A.A., Khoshkholgh M.J., Morsali A.* // Spectrochim. Acta, Part A. – 2008. – **71**. – P. 1341 – 1347.
28. *Eshtiagh-Hosseini H., Housaindokht M.R., Beyramabadi S.A., Tabatabaei S.H.M., Esmaeili A.A., Khoshkholgh M.J.* // Spectrochim. Acta, Part A. – 2011. – **78**. – P. 1046 – 1050.
29. *Beyramabadi S.A., Morsali A., Shams A.R.* // J. Struct. Chem. – 2015. – **56**. – P. 243 – 249.
30. *Eshtiagh-Hosseini H., Beyramabadi S.A., Morsali A., Mirzaei M., Salimi A.R., Naseri M.A.* // J. Struct. Chem. – 2013. – **54**. – P. 1063 – 1069.
31. *Beyramabadi S.A., Morsali A., Khoshkholgh M.J., Esmaeili A.A.* // Spectrochim. Acta, Part A. – 2011. – **83**. – P. 467 – 471.

32. *Beyramabadi S.A., Morsali A., Khoshkholgh M.J., Esmaeili A.A.* // J. Struct. Chem. – 2012. – **53**. – P. 460 – 467.
33. *Hatop H., Ferbinteanu M., Roesky H.W., Cimpoesu F., Schiefer M., Schmidth H.G., Noltemeyer M.* // Inorg. Chem. – 2002. – **41**. – P. 1022 – 1025.
34. *Johnson M.K., Cannon R.D., Powell D.B.* // Spectrochim. Acta, Part A. – 1982. – **38**. – P. 307 – 315.
35. *Sanmartín J., García-Deibe A.M., Fondo M., Navarro D., Bermejo M.R.* // Polyhedron. – 2004. – **23**. – P. 963 – 967.
36. *Bader R., Nguyen-Dang T., Tal Y.* // Rep. Prog. Phys. – 1981. – **44**. – P. 893 – 948.
37. *Bader R.F.* Atoms in molecules. – Wiley Online Library, 1990.
38. *Keith T., Bader R., Aray Y.* // Int. J. Quantum Chem. – 1996. – **57**. – P. 183 – 198.
39. *Cortés-Guzmán F., Bader R.F.* // Coord. Chem. Rev. – 2005. – **249**. – P. 633 – 662.
40. *Bader R.F., Carroll M.T., Cheeseman J.R., Chang C.* // J. Am. Chem. Soc. – 1987. – **109**. – P. 7968 – 7979.
41. *Bader R., Stephens M.* // J. Am. Chem. Soc. – 1975. – **97**. – P. 7391 – 7399.
42. *Macchi P., Sironi A.* // Coord. Chem. Rev. – 2003. – **238**. – P. 383 – 412.
43. *Cremer D., Kraka E.* // Angew. Chem. – 1984. – **23**. – P. 627 – 628.
44. *Molina J.M., Dobado J., Heard G.L., Bader R.F., Sundberg M.R.* // Theor. Chem. Acc. – 2001. – **105**. – P. 365 – 373.
45. *Bader R.* // Int. J. Quantum Chem. – 2003. – **94**. – P. 173 – 177.